Tidal-Fluvial and Estuarine Processes in the Lower Columbia River: I. Along-Channel Water Level Variations, Pacific Ocean to Bonneville Dam

David A. Jay · Keith Leffler · Heida L. Diefenderfer · Amy B. Borde

Abstract This two-part paper provides comprehensive time and frequency domain analyses and models of along-channel water level variations in the 234-km-long Lower Columbia River and Estuary (LCRE) and documents the response of floodplain wetlands thereto. In Part I, power spectra, continuous wavelet transforms, and harmonic analyses are used to understand the influences of tides, river flow, upwelling and downwelling, and hydropower operations ("power-peaking") on the water level regime. Estuarine water levels are influenced primarily by astronomical tides and coastal processes and secondarily by river flow. The importance of coastal and tidal influences decreases in the landward direction, and water levels are increasingly controlled by river flow variations at periods from ≤1 day to years. Water level records are only slightly nonstationary near the ocean, but become highly irregular upriver. Although astronomically forced tidal constituents decrease above the estuary, tidal fortnightly and overtide variations increase for 80–200 km landward, both relative to major tidal constituents and in absolute terms. Near the head of the tide at Bonneville Dam, strong diel and weekly fluctuations caused by power-peaking replace tidal daily (diurnal and semidiurnal) and fortnightly variations. Tides account for 60–70 %, river flow and seasonal processes 5–20 %, and weather 2–4 % of the total variance in the seaward 60 km of the system. In the landward 70 km of the LCRE, seasonal-fluvial variations account for 80–90 % of the variance, power-peaking 1–6 %, and tides <5 %. In Part II, regression models of water levels and inundation patterns are used to understand the distribution of floodplain wetlands, and a system zonation is defined based on bedrock geology, hydrology, and biota.

Keywords Estuarine processes · Floodplain · Hydropower impacts · Nonstationary tides · Tidal river · Tides · Water levels · Wetlands

D. A. Jay (✉) · K. Leffler
Department of Civil and Environmental Engineering, Portland State University, P.O Box 751, Portland, OR 97207-0751, USA
e-mail: djay@cecs.pdx.edu

K. Leffler
e-mail: leffler@cecs.pdx.edu

H. L. Diefenderfer · A. B. Borde
Marine Sciences Laboratory, Pacific Northwest National Laboratory, 1529 West Sequim Bay Road, Sequim, WA 98382, USA

H. L. Diefenderfer
e-mail: heida.diefenderfer@pnnl.gov

A. B. Borde
e-mail: amy.borde@pnnl.gov

Introduction

The lower Columbia River and Estuary (LCRE; Fig. 1) has highly variable water levels that are influenced by tides, river flow, atmospheric forcing, and hydropower operations ("power-peaking"). These factors produce distinctive though overlapping spectral signatures and spatial patterns in water levels which, in turn, influence ecosystem processes. Like all large river floodplains, the hydrologic regime varies along multiple spatial gradients that can be broadly conceptualized as either lateral (normal to the thalweg) or longitudinal (along-channel) from the river mouth landward (Junk and Wantzen 2004). This variation in water level has a strong role in controlling the development of estuaries and tidal freshwater wetlands (Bunn and Arthington 2002; Wolanski 2007; Barendregt et al. 2009). The purposes of this two-part study are to analyze the water level regime of the LCRE, define the transformation of the water level spectrum from the ocean to the head of the
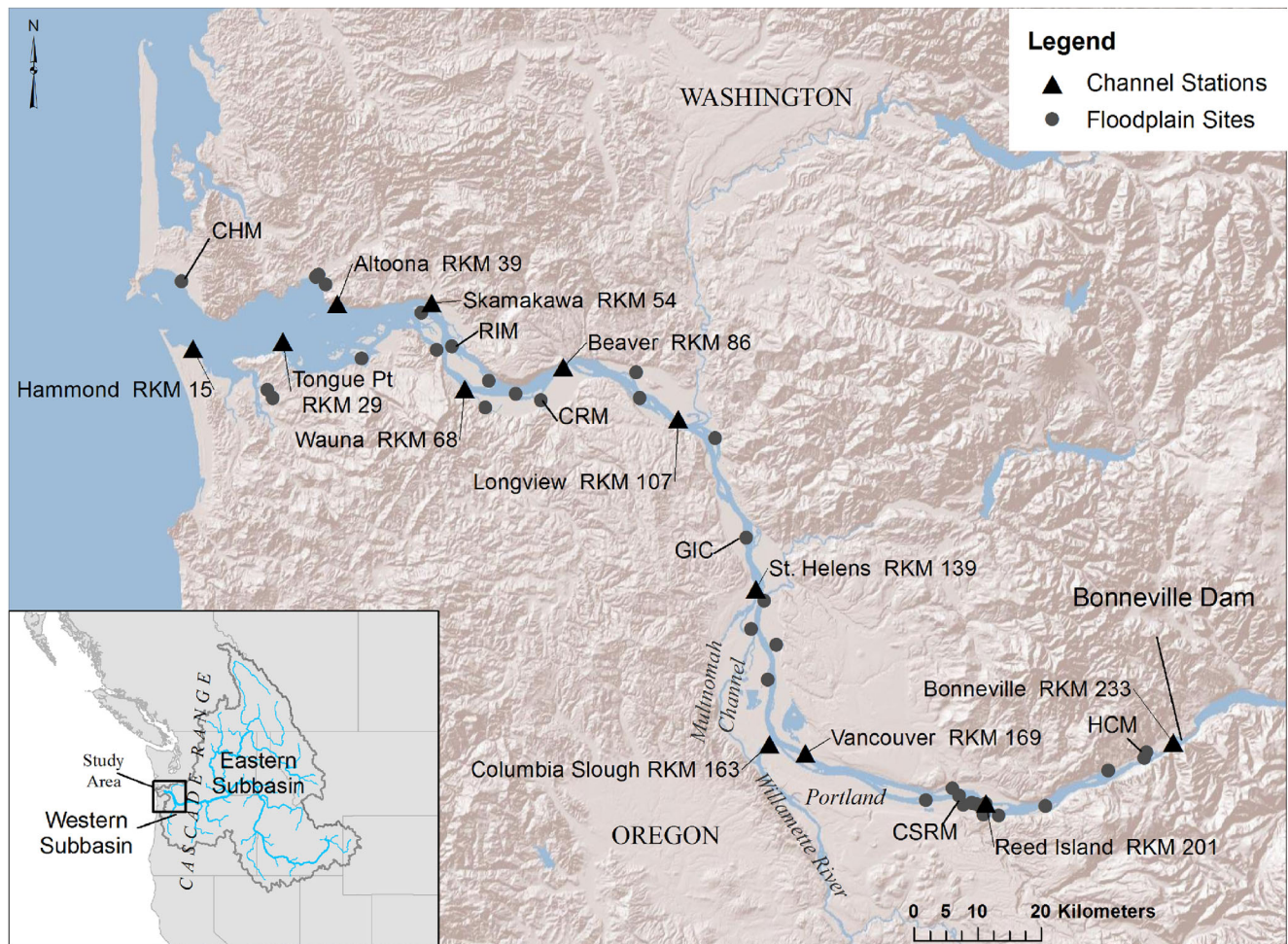
Fig. 1 Lower Columbia River and Estuary (LCRE) location map, with river kilometer (rkm) designations for channel stations [*triangles*]; floodplain stations referred to in the text, are shown as *dots*

tide, to understand the distribution and inundation of flood-plain wetlands, and define system zonation. Hydrology is the driver of primary production and the floodplain food web, which are the basis of fish production (Welcome 1979). To provide an ability to predict the effects of climate change and hydropower system operations on the distribution of these important ecosystems and to inform current wetland restoration efforts, we need to develop an understanding of processes and transition zones in the combined estuary, tidal river, and floodplain system and knowledge of the spatial variation of controls on hydrologic processes. A better understanding of these issues would be valuable both for the LCRE and for highly developed river systems around the world.

Such tidal-fluvial processes have been studied in large rivers worldwide. These include the Amazon River in Brazil which has both very large tides and flow (Amphlett and Brabben 1991; Hida et al. 1998; Gallo and Vinzon 2005; Bezerra et al. 2008); the Berau and Mahakam deltas in Indonesia, where modeling similar to ours has been carried out (Buschman et al. 2010; Sassi et al. 2011); the Thames in England, where growth of the tides (Amin 1983) has been

even stronger than in the LCRE (Jay et al. 2011); the Yangtze River in China, where flows are larger than in the LCRE (Yixin et al. 2001; Jiao et al. 2006); and the Gironde estuary in France, where tides are larger and flow much less than in the LCRE (Castaing and Allen 1981; Mikhailova and Isupova 2006). In North America, tidal-fluvial forcing has been studied in several systems including, in Canada, the Fraser River, the system most similar to the LCRE (LeBlond 1978; Stronach and Murty 1989; Levings et al. 1991; Kostachuk 2002) and the St. Lawrence (Godin 1999), similar to the Columbia in flow, but without daily power-peaking. In the USA, the Delaware (Parker 1991; DiLorenzo et al. 1993) and the Hudson in New York (Smith et al. 2009), where flows are much smaller than in the LCRE, have been studied. Backwater effects have been analyzed in the Mississippi, a microtidal system with higher river flows than the Columbia (Nittrouer et al. 2012). Backwater theory is not especially relevant in the LCRE, because of the role of tides and bedrock constraints in determining water levels. Power-peaking effects have been analyzed in nontidal contexts in the Colorado River in the western USA (Wiele and Smith 1996; White et al. 2005)

and the Alto Adige in Italy (Zolezzi et al. 2009). In terms of methods, the studies by Buschman et al. (2010) and Sassi et al. (2011) are closest to the present study, because all three use models based on continuous wavelet transform (CWT) analyses of water levels, an approach stemming from Jay and Flinchem (1997) and Kukulka and Jay (2003a, b).

The LCRE extends 234 km from the Pacific Ocean to Bonneville Dam, built on a rapids that has formed the head of the tide since an immense landslide about 1450 AD. The 668,000-km^2 Columbia River basin consists of an Interior Subbasin east of the Cascade Mountains (providing about three fourths of the flow at the mouth) and a Western or Coastal Subbasin to the west of the range (Naik and Jay 2005; providing about one fourth of the flow). Columbia River flows, measured daily since 1878 at The Dalles (rkm-310), varied naturally from ~1,000 to 35,000 m^3 s^{-1}. (River channel locations are given in river kilometers or rkm, measured from the seaward end of the jetties at the river mouth, which is rkm-0.) The present, regulated flows vary from about 2,000 to 16,000 m^3 s^{-1}; the 1991–2011 average flow was 5,010 m^3 s^{-1}. The Columbia Interior Subbasin flow, ~97 % of which is measured at The Dalles, is fed primarily by spring snowmelt. The peak spring flow or "freshet" now occurs in May; before 1900 the peak typically occurred in June. In addition to long-term changes in flow seasonality due to earlier snowmelt, multiple uses have reduced spring freshet amplitude by ~45 %: irrigation withdrawal, reduced precipitation, and flow regulation for flood control and power generation (Naik and Jay 2011). The extent of saltwater intrusion, governed by river flow and tidal range, is usually 10 to 40 km from the ocean (Jay and Smith 1990).

The Willamette River, the largest Western Subbasin tributary, enters the Columbia River at Portland, 160 km from the ocean, and accounts for about 40 % of the Western Subbasin flow. It is tidal for 26 km to Oregon City. Western Subbasin flows respond much more rapidly to precipitation because snow-pack storage is less than in the Interior Subbasin, and flows are less regulated. The largest floods represent winter rain-on-snow events (Jay and Naik 2011). Willamette River flows over the 1991–2011 period ranged from 140 to 11,900 m^3 s^{-1}; the latter in a brief flood in February 1996, the largest since 1964. The mean flow over the same period was 954 m^3 s^{-1}. The total flow through the LCRE is the sum of that from the Interior and Western Subbasins, best represented by the gauge at Beaver (rkm-87), which captures an average of ~97 % of the total flow to the ocean. Over the 1991–2011 period, the minimum, maximum, and mean flows at Beaver were 1,800, 24,500, and 6,570 m^3 s^{-1}, respectively.

Previous studies of tidal-fluvial interactions in the LCRE based on harmonic analysis methods and related models were carried out by Giese and Jay (1989) and Jay et al. (1990). Harmonic analysis is used here (along with conventional power spectra) to provide a time-average view of the system processes.

However, because these methods, designed for stationary processes, cannot capture the highly nonstationary processes observed in the system, Jay and Flinchem (1997) developed CWT tidal analysis for nonstationary tides. ("Nonstationary" is used here to refer to processes whose statistical properties are time variable, so that analysis results vary with the time period analyzed.) CWTs are used herein to quantify time variability in system processes, including the damping of LCRE tides and generation of overtides (tidal energy at multiples of the basic tidal frequencies, analogous to musical overtones) as a function of river flow velocity that varies in space and time. Kukulka and Jay (2003a, b) used CWT methods and developed a regression analysis approach to parameterize tidal-fluvial interactions based on a theoretical tidal propagation model developed by Jay (1991). Jay et al. (2011) extended the Kukulka and Jay regression approach to the analysis of historical changes in tidal datum levels.

Part I analyzes, in the time and frequency domains, water level records (1991–2011) from 12 tide stations along the mainstem river ("channel stations") and selected wetland pressure gauges ("floodplain stations") and parses water level variance by source mechanism. We seek to understand what factors control water level variations in different parts of the system, and how the frequency distributions of flow processes change along the system, focusing on the along-channel perspective. Because of the length of the system and diversity of forcing factors, the water level regime changes drastically between the ocean and the head of the tide at the most seaward dam (Bonneville Dam at rkm-234).

Part II of this study represents with simple regression models (Jay et al. 2011) the dominant processes influencing water levels, hindcasts 21-year inundation distributions for channel and floodplain stations, and describes the effects of water level variations on the distribution of floodplain wetlands. A related study (Borde et al. 2012; Sagar et al. 2013) analyzes plant community, environment, and water level data from >50 tidal wetlands throughout the LCRE and results, along with our water level analyses, form the basis for the analysis of wetlands in Part II. The LCRE has been variously described in terms of estuarine, tidal-fluvial, and fluvial-dominated hydrologic zones (Sherwood et al. 1990; Jay and Smith 1990; Simenstad et al. 2011). A zonation of the system is provided in Part II, based in part on the distribution of the processes that control water levels. Here, we will refer to the system landward of Beaver (rkm-87) as the "tidal river," while more seaward reaches are the "estuary."

Methods

The water level, river flow, and atmospheric data on which our analysis is based cover a 21-year period, January 1991 to November 2011. This period was chosen to represent "the present" in terms of hydrology and flow management and to

be long enough to encompass a large dynamic range of river-flow conditions, including winter freshets in 1996 and 1997, several moderate to large spring freshets (1997, 1999, 2008, and 2011), and very dry conditions in 1992, 1994, and 2001. In terms of tidal forcing, this period also covers slightly more than one 18.6-year nodal cycle. To relate the water levels observed at the 12 channel stations (Fig. 1) to wetland inundation patterns (Part II), water level data collected 2005–2010 through 35 pressure gauge deployments (1–2-year duration) at wetland stations were analyzed, using both time and frequency domain methods.

Water Level Data

Hourly data for the 1991–2011 period from nine tide gauges in or closely adjacent to deep water were obtained from the responsible agencies (Fig. 1 and Table 1). These "channel" stations were analyzed to understand tidal conditions in the main channel. The only long-term, estuarine tide station is Tongue Point (Astoria, Ore). Therefore, data from two stations occupied by NOAA-NOS during the 1980s were also included in the analysis: Hammond and Altoona. Because there are no long-term tide gauges between Vancouver at rkm-169 and the gauge nearest Bonneville (rkm-233), data from a pressure gauge deployed for 2 years close to open water at Reed Island (rkm-201) were also used; harmonic analyses of these data suggest that they reflect channel conditions.

Hobo® pressure gauges (Onset Computer Corporation) were deployed at 35 floodplain sites for periods of 1–2 years; see Fig. 1 and Table 2 for floodplain stations discussed in Part I and Electronic Supplementary Material (ESM) Table 1 for all floodplain stations analyzed. Variables were sampled every 30 or 60 min, though some stations have gaps due to very low water levels. Sensor elevations were determined using

Trimble real-time kinematic global positioning system (RTK) methods. Pressure data were corrected for atmospheric pressure variations and converted to elevation relative to the North American Vertical Datum of 1988 (NAVD88) or the Columbia River Datum (CRD) as needed. Hourly atmospheric pressure data were obtained from the National Climate Data Center (http://cdo.ncdc.noaa.gov/pls/plclimprod/poemain.accessrouter/). Wetland pressure-gauge time-series data are further discussed in Part II.

Frequency Domain Analyses

The water level regime of tidal rivers is complex and statistically nonstationary (Jay and Flinchem 1997). River flows vary over time and strongly modify tides through friction (LeBlond 1978; Horrevoets et al. 2004), and there is energy at seasonal, annual, and interannual time scales because of variations in river flow. As with any nonstationary signal, it is useful to employ more than one analysis tool; we focus on analyses of subdaily to annual fluctuations using harmonic analysis, power spectra, and CWT methods. A harmonic analysis defines average values of phases and amplitudes of tidal constituents, but provides no direct information regarding nontidal processes. A power spectrum defines the time-average of the frequency content of water level time series at narrowly spaced frequencies, which do not, however, necessarily include all relevant tidal frequencies. A CWT analysis defines the time-varying frequency content of a signal, but with reduced frequency resolution relative to the other two methods. There is no method available that is especially adapted to the peculiarities of tides at floodplain stations with truncated low waters; in power spectra and harmonic analyses, the truncation of low waters adds energy at high frequencies that, while interpretable, is in some sense also artificial.

Table 1 Long-term channel stations

Name	Data sources	rkm	Data used[a]	LOR, hours	% Complete	CRD on NAVD88, m
Hammond	NOS	15	1982–1989	59,496	89.1	−0.143
Tongue Point	NOS	29	1991–2011	183,386	100	−0.182
Altoona	NOS	39	1981	5,040	100	0.149
Skamokawa	Corps <2002, NOS	54	1991–2011	183,386	94.0	0.273
Wauna	Corps <2002, NOS	67	1991–2011	183,386	95.7	0.442
Beaver	USGS	87	1991–2011	183,386	95.5	0.63
Longview	Corps <2002, NOS	107	1991–2011	183,386	96.3	0.88
St Helens	Corps <2002, NOS	139	1991–2011	183,386	94.6	1.262
Columbia Slough	USGS	154	1991–2011	183,386	95.2	1.336
Vancouver	Corps <2002, NOS	171	1991–2011	183,386	95.6	1.634
Reed Island	PNNL	198	2007–2009	19,248	91.2	2.21
Bonneville	USGS	233	1991–2011	183,386	99.8	3.59

LOR length of record, *NOS* National Ocean Service, *USGS* US Geological Survey, *Corps* US Army Corps of Engineers

[a] For the 1991–2011 stations, data from 1991/1/1 to 2011/11/30 were used

Table 2 Floodplain stations mentioned in the text

rkm	Station name	Code	Deployment	Retrieval	LOR (days)	% Good
12	Chinook Marsh	CHM	August 17, 2008	August 18, 2009	365	100
61	Ryan Island Marsh	RIM	July 23, 2009	August 10, 2010	383	100
80	Clatskanie River Marsh	CRM	August 18, 2008	July 24, 2009	340	100
98	Coal Creek Riparian	CCR	July 20, 2008	August 8, 2009	384	90
131	Goat Island Marsh	GIC	August 18, 2008	August 9, 2009	356	100
195	Current Sandy River Mouth	CSRM	September 20, 2008	September 19, 2009	364	100
229	Hardy Creek	HCM	July 23, 2008	July 26, 2009	368	100

LOR length of record

Harmonic Analysis

Tidal harmonic analysis, a least-squares fitting procedure, is normally used for determination of tidal constituent phases and amplitudes in systems in which, unlike a tidal river, tidal properties are stationary (Jay and Flinchem 1999). A robust least squares fitting procedure (Huber 1996; Leffler and Jay 2009) is used here to compute tidal phases and amplitudes and confidence intervals with a variant of the T_Tide harmonic analysis code (Pawlowicz et al. 2002). Annual (8,761 h) harmonic analyses with 67 constituents were used here to approximate the average tidal properties at channel stations with long records. Even though T_Tide accommodates gaps in data, some floodplain stations did not have a full year of valid data, and the analysis period was accordingly shortened. To examine seasonal variations in tidal properties, overlapping (at 7-day intervals) 761-h harmonic analyses with 37 constituents were used. Use of such a short window or LOR limits the frequency resolution especially given the high levels of nontidal variance (mainly fluvial) present. For both types of analysis, only constituents that passed T_Tide's significance test (based on each constituent's emergence from the background noise spectrum) were used. At upriver stations where the tides are small and very irregular, amplitudes and phases of some constituents were found to be not significant (signal to noise ratio <2).

Spectral Analysis

The power spectrum defines the average frequency content of a time series. Power spectra were calculated with the objective of resolving processes with periods between 1 year (annual band) and 2 h (the Nyquist frequency cut-off for hourly data). In raw form, the power spectrum is the squared amplitude (or energy) per unit frequency of a signal as determined by a Fourier transform (Emery and Thomson 1997). For comparison to CWT analyses, the raw power spectral outputs are multiplied by frequency, to give an "energy-conserving" power spectrum. Thus, for water level measurements in meters, the power spectra are reported in meters squared. Power spectra were calculated for hourly water level time series and for the various forcing

functions that influence water levels: river flow, coastal processes (upwelling and downwelling), and the astronomical tidal potential.

Upwelling and downwelling lower and raise (respectively) estuarine water levels due to their impacts on continental shelf water levels. These effects are represented by the offshore component of the Coastal Upwelling Index or CUI in $10 \ m^2 \ s^{-1}$ (available at 6-h intervals, see www.pfeg.noaa.gov/products/PFEL/modeled/indices/upwelling/ for details). Positive values of the offshore component of CUI represent upwelling and the offshore transport of water caused by alongshore (geostrophic) windstress. CUI values were interpolated between {45° N, 125° W} and {48° N, 125° W} to 46° N (near the mouth of the Columbia River).

The tidal potential is the astronomical tidal forcing V in square meters per square second. As described by Cartwright and Edden (1973), V is determined using a program provided by Dr. Richard Ray of the National Aeronautical and Space Administration (Ray, personal communication). If the water surface was in perfect equilibrium with astronomical forcing, the surface elevation would be V/g, where g is the gravitational acceleration $g=9.81 \ m \ s^{-2}$. Thus, the calculated spectra are of V/g and have units of meters. Spectral methods are further discussed in ESM-1a.

Continuous Wavelet Transform Analysis (CWT)

The CWT optimizes, in terms of the Heisenberg uncertainty principle, the recovery of time-varying frequency information from a time series by the use of a filter bank. The length of filters and duration of their application vary inversely with frequency; i.e., low frequencies have long filters applied at long time intervals, and high frequencies have short filters applied at short time intervals (Flinchem and Jay 2000). The advantages of the CWT over harmonic analysis (which has a fixed analysis period for all frequencies) are as follows: (1) more accurate results during periods of fluctuating tidal properties and (2) better temporal resolution of variations in frequency content, because filter length and overlap are tuned for each frequency. Like a harmonic analysis, but in contrast to a power

spectrum, the CWT transform can be calculated from gappy data. Also, CWT analyses abandon tidal constituents (e.g., O_1 and K_1 within the diurnal species, and semidiurnals M_2 and S_2), in favor of the more physical tidal species (e.g., the diurnal and semidiurnal bands, which we call D_1 and D_2 here). A CWT is calculated through convolution of a time series with a scaled wavelet. A wavelet is a function with zero mean, finite energy and duration, and a narrow frequency response at a particular scale (Jay and Flinchem 1997). A wavelet filter bank, consisting of the frequencies (four per power of two in frequency) between D_8 (~8 day^{-1}) and 1/29 day^{-1}, was used for the analysis of the short (~1–2 years) floodplain records. For analysis of the nine channel stations with long records, frequencies down to 1/439 day^{-1} were used. The frequency spacing is somewhat irregular to accommodate processes of interest; see Table ESM-2 for a partial listing of the 53 frequencies used. CWT results are conventionally plotted as amplitude scaleograms (contour plots of amplitude as a function of time and frequency), with the same units as the input data. See ESM 1b for further details.

Water Level Variance: Spatial Patterns and Mechanisms

Spatial patterns of water level variance and their causes provide valuable insights into hydrologic controls on vegetation distribution, the indicators of which include the sum exceedance value (Gowing and Spoor 1998; Borde et al. 2012; Sagar et al. 2013) used in Part II. To separate the effect of the diverse forcing factors and provide an along-channel view of variations in controlling processes, the variance (in m^2) in each CWT band was calculated. For each frequency band, variance=½(RMS)^2 of the wavelet amplitude time series for that band (RMS=root mean square). Variances for related bands were summed to give the total energy level for each forcing process: tides, diel and weekly power-peaking, weather, seasonal river flow, and inter-annual river flow variations. The CWT bands assigned to each process, corrections for band overlap, and other details are described in ESM-1c. Because of the short LOR for floodplain stations, river-flow variance at periods greater than ~29 days could not be estimated for these stations.

Results

Here, we examine the LCRE water levels in both the time and frequency domains to understand and separate variance due to forcing by tides, river flow, coastal processes, and power-peaking. This descriptive view of the complex time-space variability of the system is needed to provide context for the regression analyses and comparison to the distribution of wetlands in Part II. The spatial variations in frequency content and energy levels then potentially inform our ability to predict

the distribution of wetlands under climate change and hydro-power operations scenarios—inundation is daily in the estuary but evolves to seasonal upriver. Moreover, alterations in the flow cycle due to flow regulation, diversion, and climate change have altered the annual flow cycle (Jay and Naik 2011), modified the tidal regime (Jay et al. 2011), and added (as described below) power-peaking disturbance to the water level spectrum.

Time-Space Variations of Water Levels

The character of water level variations changes dramatically along the length of the LCRE, and it is useful to consider these changes as a continuum, from control of water levels by tidal and coastal processes near the ocean to control by fluvial processes and power-peaking upriver. Figure 2 shows 60-day time series of water levels during and after the 2009 spring freshet for five channel and five floodplain stations, along with Bonneville Dam outflow and Willamette River flow. Near the river mouth at Tongue Point (rkm-29), water level variations are regular and largely tidal. The nonstationary component consists mostly of subtidal variations driven by coastal processes (especially upwelling and downwelling and related atmospheric pressure variations), and river-flow has only a small impact on tidal ranges and water levels. Water level variations at Beaver (rkm-87) are superficially similar to those at Tongue Point, but with smaller tidal amplitudes. However, the spring freshet raises water levels by 0.5–1 m, and the tidal wave has become somewhat asymmetric through energy transfer to overtides and subtidal frequencies—the duration of rising tide is less than that of the falling tide. A more subtle difference is that the diurnal inequality (difference between successive tides or successive low tides) is diminished at Beaver relative to Tongue Point.

Landward of Beaver, tidal variability decreases, tidal range varies inversely with river flow, and water levels are very irregular (Fig. 2). At St Helens (rkm-139) and Vancouver (rkm-169), tides are greatly suppressed, and mean water level (MWL) is elevated by 1.5–3.2 m during the freshet (first half of the record); this increase in elevation is greater than the maximum tidal range. Tides are stronger after 1 July as flow and MWL drop. Near Bonneville (rkm-233), it is difficult to discern the tidal variability, and freshet water levels are even more elevated, by 2.8–5.3 m. The 2009 freshet was weaker than average, and MWL is usually even more elevated and tides smaller during the peak flow period. At the tidal river stations (Beaver to Vancouver), there is considerable tidal monthly variability at ~13–15 and ~29-day periods–MWL (which corresponds to river stage as defined in a non-tidal environment) is systematically higher in the tidal river on spring than on neap tides. This variability is also suppressed somewhat by the freshet, from St Helens landward.

Fig. 2 Columbia River inflow at Bonneville Dam (hourly) and from the Willamette River at Portland (daily) (*top row*), with time series of hourly tidal heights (hts) relative to CRD for (*at left*) five channel stations and (*at right*) five floodplain stations: Chinook Marsh (CHM), Clatskanie River Marsh (CRM), Goat Island (GIC), Current Sandy River Mouth (CSRM), and Hardy Creek Marsh (HCM). Station locations are shown in Fig. 1; elevations are in m on CRD. Floodplain stations were chosen to roughly correspond to channel stations in terms of along-channel position. Water levels are from a 60-day period during the 2009 spring freshet, when Bonneville flows reached ~10,500 m^3 s^{-1} and Willamette River flows peaked at 750 m^3 s^{-1}. Note the truncation of low waters at the three seaward floodplain stations. Low waters are truncated at the more landward floodplain stations during low-flow periods
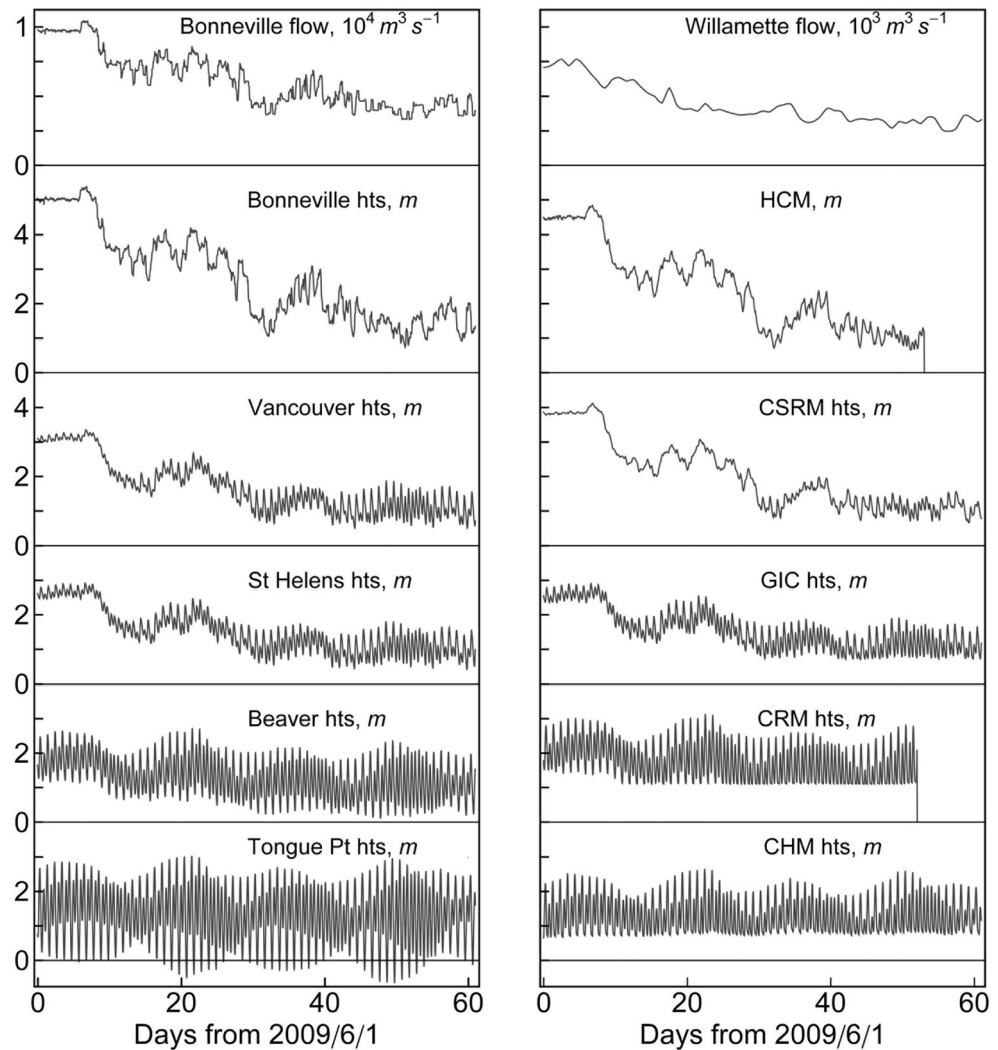
Water levels at floodplain stations show the same along-channel progression from tidal to fluvial dominance in the upriver direction (Fig. 2). However, floodplain water level variations are more complex due to distortion and dissipation of the tides in shallow water and the effects of sills or generally higher elevation channel bottoms that truncate low waters at a base level at all stations. Hardy Creek Marsh (HCM, rkm-229), totally isolated from the river during lower flow periods, is an even more extreme case. The neap-spring percentage change in water depth is higher in shallow water, and the truncation of low waters may decrease or disappear during neap tides. Thus, tidal monthly variability may be stronger than or quite different from nearby channel stations. Also, tidal river floodplain stations like Goat Island Marsh (GIC, rkm-131) may show truncation of low waters only during the low-flow season, whereas estuarine sites like Chinook Marsh (CHM, rkm-12) exhibit truncated low waters all year. Clatskanie River Marsh (CRM, rkm-80) is an intermediate case, with truncation during low-to-medium flow conditions.

The Frequency Structure of Water Level Variations

Power Spectral Results

Power spectra and CWT analyses are often used together, because the former provides a high-resolution (in frequency) view of the average frequency content of a signal, while the latter resolves time variations in frequency content, but at a lower frequency resolution. Harmonic analysis can then used to quantify specifically tidal processes. We begin by examining the time-averaged frequency content using power spectra that cover the frequency range from ~1 year^{-1} to D_{12}. Paired power spectra (Fig. 3), along the gradient from near the river mouth to Bonneville, provide a means of comparing nearby stations or related processes.

Tidal Potential, Coastal Upwelling Index, and Tongue Point (rkm-29) Water Levels. The spectrum of the tidal potential gives the frequency structure that would be observed if water levels were in equilibrium with astronomical tidal forcing and
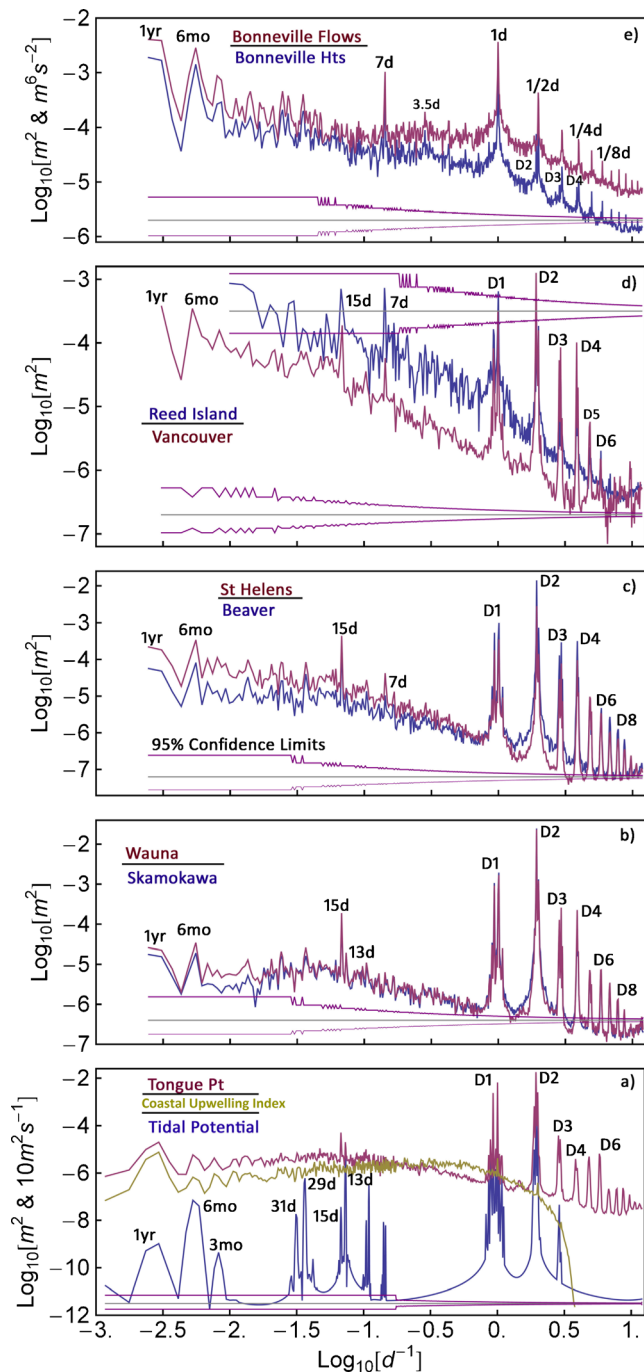
Fig. 3 Power spectra (1 cycle year^{-1} to D$_{12}$) for channel stations and forcing functions: **a** Tongue Point (rkm-29), astronomical tidal potential, and CUI; **b** Skamokawa (rkm-54) and Wauna (rkm-68); **c** Beaver (rkm-86) and St Helens (rkm-139); **d** Vancouver (rkm-169) and Reed Is. (rkm-201); and **e** Bonneville and Bonneville hourly flow (rkm-233 and rkm-234). The order of the labels in each panel identifies the spectra

unaffected by other processes (Fig. 3a). There is astronomical forcing in the D$_1$ to D$_3$ bands, at tidal monthly frequencies (13–31 days) and at ~3, 6, and 12 months. The CUI spectrum is almost flat and has energy at all frequencies resolved by the

6-h data. The only significant peaks are at 6 months and 1 year. Regression analyses (Part II) indicate that a change in CUI during summer upwelling of +0.2 (in units of 10 m^2 s^{-1}) causes a drop in water level at Tongue Point of 0.13 m. A large storm resulting in a change of CUI of −10 m^2 s^{-1} would cause a predicted rise of 0.64 m at Tongue Point; however, atmospheric pressure variations also influence water levels, and storm surges in the estuary occasionally exceed 1 m. Thus, we expect the Tongue Point water level spectrum to reflect the broad range of frequencies seen in the CUI and atmospheric forcing in general.

Tongue Point is the most seaward station for which long records are available. Tongue Point water levels have energy at the frequencies of the tidal forcing and at other frequencies as well. The D$_1$ and D$_2$ tidal bands follow fairly closely the astronomical forcing, with the D$_2$ band stronger than D$_1$. The overtide bands (D$_3$ to D$_{12}$ and beyond) are weak or absent in the tidal potential; they are caused almost entirely by shallow water frictional interactions. The influence of nontidal, coastal, and fluvial motions on Tongue Point water levels is emphasized by the almost continuous frequency distribution at subtidal frequencies. This background "noise" level is 2–5 orders of magnitude above the level of the tidal potential spectrum at most frequencies. At subtidal frequencies, only the 13–15-day tidal peaks emerge from the background noise.

Skamokawa (rkm-54) and Wauna (rkm-68). Water levels at these two stations in the upper estuary are similar to Tongue Point, but the overtide and 13–15-day peaks are stronger relative to the tides and/or more distinct from the background, due to nonlinear friction (Fig. 3b). Also, the D$_1$ tide is weaker relative to D$_2$, while overtides are stronger than at Tongue Point. The 6- and 12-month peaks are larger at Wauna than at Skamokawa and more distinct from each other than at Tongue Point, due to the growing influence of the annual flow cycle and because coastal processes are less prominent here than in the estuary.

Beaver (rkm-87) and St Helens (rkm-139). These two stations encompass the seaward 53 km of the ~142-km long tidal river. Overtides (D$_3$ to D$_{12}$) and low-frequency bands (tidal monthly to annual) increase in prominence (relative to D$_1$ and D$_2$) as D$_1$ and D$_2$ continue to transfer energy to higher and lower frequencies (Fig. 3c). The 15-day band is now very prominent and the 6- and 12-month peaks are of growing importance. For the first time, the 7-day power-peaking band is evident, if only marginally significant at St Helens. The background spectrum between the tidal and 6-month peaks is now more energetic below 15 days than above 15 days (in contrast to estuarine stations). This change indicates that fluvial processes (stronger below 15 days) are more important than coastal processes in the tidal river.

Vancouver (rkm-169) and Reed Island (rkm-201). Progressing further landward in the tidal river, the power spectrum at Vancouver (Fig. 3d) continues the trends evident in Fig. 3c, but the 6- and 12-month peaks are stronger than further seaward; D_2 is stronger than D_1, as at all stations further seaward. Reed Island is the first station at which diel power-peaking makes the D_1 peak stronger than D_2; the background "noise" level due to river flow variations is very red (with increasing energy at low frequencies) and markedly higher than at Vancouver. The 7-day power-peaking and 15-day tidal monthly peaks are as energetic as the diel band.

Bonneville (rkm-233) and Bonneville hourly flow (rkm-234). The rock slide ("The Cascades") on which Bonneville dam is built was the natural head of the tide, but most of what appears to be tidal energy at Bonneville is actually diel power-peaking and its harmonics (Fig. 3e). The multiple D_1 peaks at more seaward stations have been replaced by a single diel peak. The power-peaking harmonics (periods of ½ day, ¼ day, etc.) arise because the diel cycle is not a smooth sinusoid but contains sharp ramps up and down. The high background noise level is caused by the irregular timing of hydropower operations. The diel peak is also much stronger than the 12-h peak, whereas tidal D_1 is always smaller than tidal D_2 at more seaward stations. Although tidal frequencies are present in the 1/2- to 1/8-day peaks to the left (low frequency) side of the main peak in each case, they are always weaker than the nontidal peak. The relatively lower frequency of the tidal peaks stems from the fact that M_2, the main semidiurnal constituent, has a period of 12.42 h rather than 12 h, so that its frequency is less than that of the 12-h peak, and this difference is reflected in the overtides. The 7-day peak is strong, no 15-day peak is evident, and there is a small (but not significant) 3.5-day peak.

The power spectra in Fig. 3 use 9.3–18.6 years of data to resolve seasonal and annual cycles, except for Reed Island, where the short LOR limits resolution of low frequencies. Seasonal and annual variations cannot be resolved in the spectra of the 1-year floodplain records. However, processes from tidal monthly to overtide can be resolved for floodplain stations and compared to the spectra for nearby channel stations (Fig. 4). For all paired channel-floodplain stations between the estuary (CHM, rkm-12 and Tongue Point, rkm-29) and the more landward parts of the tidal river (Vancouver, rkm-169 and Current Sandy River Mouth, CSRM, rkm-195), D_1 and D_2 are stronger at the channel station in each floodplain-channel pair, while the background energy level is higher at the floodplain station, because of the irregularity of the tides. Overtides from D_3 to D_{12} are equal to or much stronger at CHM, Clatskanie River Marsh (CRM, rkm-80), and Goat Island Marsh (GIC, rkm-131) than at the nearby channel station. This occurs because the truncation of low waters for most or all of the record gives the tidal wave the
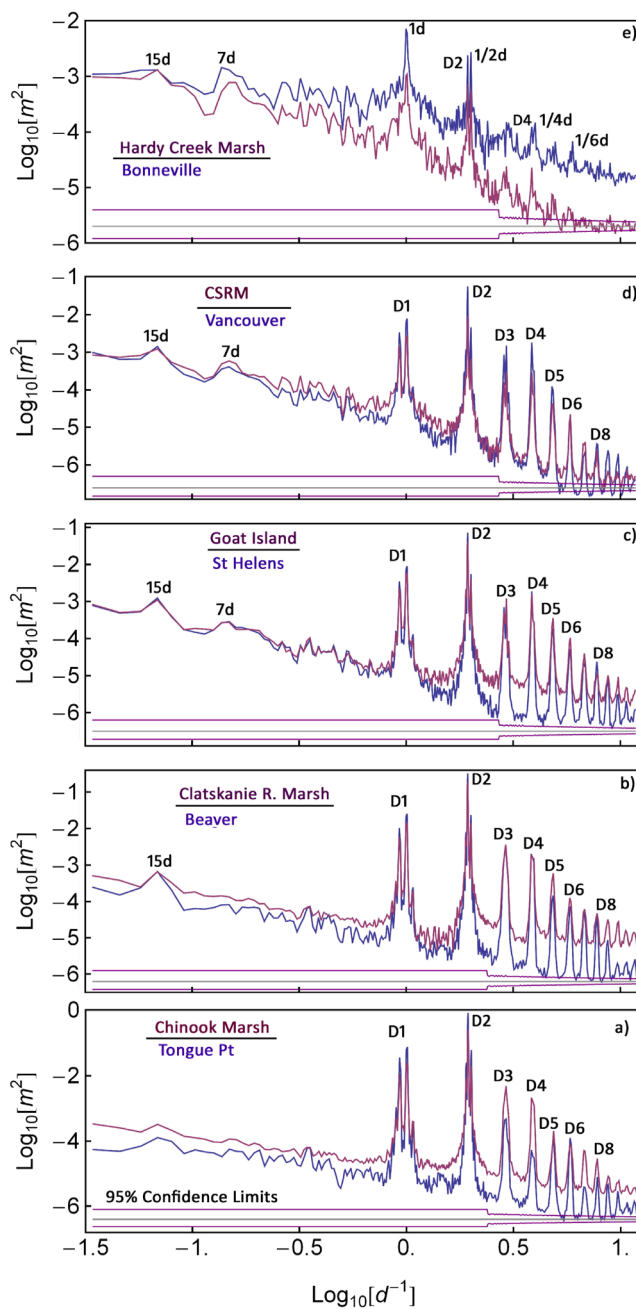

Fig. 4 a–e Tidal daily to tidal monthly power spectra for paired channel and floodplain stations. Station locations are shown in Fig. 1. All spectra have units of meters squared. The order of the labels in each panel identifies the spectra

character of a square wave, which can only be described by an infinite number of frequencies in a Fourier analysis. The tides at Vancouver are considerably larger than at CSRM (which is 26 km further landward), so the overtides are, also. The 15-day peak is present but poorly resolved (and sometimes not significant), due to the short LOR used for the floodplain spectra. Power-peaking at 7 days is present from St Helens landward. The situation at Hardy Creek Marsh (HCM, rkm-229, Fig. 4e) is complex. As at Bonneville, tidal peaks are

hidden in the background, and the diel peak is bigger at both locations than the twice-daily peak. Unlike the other floodplain stations, the background and total energy levels are smaller at HCM than at Bonneville, because HCM is totally isolated from the channel during low-flow periods.

CWT Results

Spectral plots (Figs. 3 and 4) depict average frequency content, but provide no information regarding the time variability of nonstationary river tides. CWT amplitude scaleograms provide a convenient tool for visualizing the time-varying frequency content at frequencies from D_8 down to 1 year^{-1} (Fig. 5) for forcing functions (tidal potential, CUI, and river flow) and water levels. Horizontal bands in scaleograms indicate persistence of a process at a well-defined frequency over time. Vertical bands, which typically become wider at low frequencies due to the longer length of low-frequency filters, indicate events or discrete occurrences localized in time but broad in frequency.

The Tidal Potential V/g and CUI. The scaleogram for V/g is made up of discrete horizontal bands at tidal frequencies (D_1, D_2, D_3, and tidal monthly to annual); these represent the nearly stationary nature of astronomical tidal forcing (Fig. 5a). The variable strength within tidal species bands represents the interactions of the tidal constituents within the species. In contrast, the CUI scaleogram (Fig. 5b) is mostly made up of irregular vertical streaks encompassing frequencies from ~1 to 20 days; the broad range of frequencies seen in the CUI power spectrum (Fig. 3a). Other features include the following: (a) a broad horizontal band at 6 months to 1 year that in part drives the annual sea level cycle and (b) a faint seabreeze signal in summer, visible in the diel band. The CWT scaleogram reveals, moreover, information not available in the power spectrum—that CUI variations are largest during the winter.

Tongue Point (rkm-29) and Wauna (rkm-68). The scaleogram at Tongue Point is essentially the sum of the CUI and tidal potential scaleograms. It consists of strong horizontal and weaker vertical bands, the latter in the mostly in the "storm band" with periods of 4–20 days (amplitudes up to ~0.2 m; Fig. 5c). The strongest horizontal bands, are the D_1 and D_2 tides, with amplitudes of up to 0.8 and 1.4 m, respectively. Time variability in these bands reflects variations in the tidal potential, e.g., neap-spring variations and smaller annual and interannual variations—the D_1 tides was, for example, at an 18.6-year minimum, ~11 % below average, in 1996. Overtides (nonlinear tidal constituents D_3 to D_{12} caused by frictional interactions in shallow water) at frequencies greater than D_2 are small near the ocean. Lower frequency energy at ~6–12 month^{-1} is primarily related to the annual cycle of coastal sea level. At Wauna (Fig. 5d), the D_1 and D_2 bands are

Fig. 5 Continuous wavelet transform (CWT) amplitude scaleograms (in m unless otherwise noted), 1991–2011, for forcing functions and selected channel stations: **a** astronomical tidal potential, **b** coastal upwelling index (CUI, 10 m^2 s^{-1}), **c** Tongue Point (rkm-29), **d** Wauna (rkm-68), **e** Beaver (rkm-86), **f** St Helens (rkm-139), **g** Vancouver (rkm-169), **h** Bonneville (rkm-233), **i** Bonneville flow (m^3 s^{-1}), and **j** Willamette flow (m^3 s^{-1}). Scales for individual panels are interior to the panel; the scale for height scaleograms **c** to **g** is between panels. Daily and higher frequencies cannot be computed from the daily Willamette River flow

diminished relative to Tongue Point, weather-related variance is reduced, there are clear overtide and 15-day bands, and seasonal variance is prominent. Unlike at Tongue Point, the three large freshets of the 1996–1997 period disturb the D_1 and D_2 bands.

Beaver (rkm-87), St Helens (rkm-139) and Vancouver (rkm-169). At Beaver and St Helens in the lower tidal river, tidal amplitudes are smaller and constitute a smaller part of the total signal (Fig. 5e, f). Overtides have grown, there is a strong ~13–15-day neap-spring signal, and the annual flow cycle is strong. There are more vertical streaks associated with river-flow events and considerable energy associated with seasonal river-flow variations. There is little energy evident in the 7-day power-peaking band. At Vancouver near the head of the tidal river, the trends evident at Beaver and St Helens relative to Tongue Point continue (Fig. 5g): D_1 and D_2 tides are weaker, overtides are stronger, neap-spring and seasonal variability are larger, interannual variability is more evident, and there is some energy in the 7-day power-peaking band. The annual flow cycle is much larger than the tidal signal, and the highest energy is associated with river-flow events such as occurred in February 1996.

Bonneville (rkm-233) and Bonneville Flow (rkm-234). There is little D_2 tidal energy in the Bonneville tide record (Fig. 5h). The energy in both the height and flow records (Fig. 5h, i) in the diel band is caused by power-peaking. There is also more energy in the 7-day power-peaking band than in the 13–15-day neap-spring band. There is some energy around 3.5 day associated with the irregularity and abrupt nature of weekly power-peaking. In some cases, strong weekly power-peaking is associated with strong D_1 power-peaking, but both are irregular. Because of the multiyear length of the 12-month filters, the high-flow periods in 1996 to 1999 appear as a single, long period of strong annual fluctuations.

Willamette River Flow (rkm-164). The Willamette River enters the mainstem below Vancouver, with an additional connection via Multnomah Channel that enters near St Helens. There is little subdaily flow variation, hourly flow data are not available, and the scaleogram was based on daily data (Fig. 5j). The Willamette River flow signal has persistent 6- and 12-month components and events with energy between ~2 and
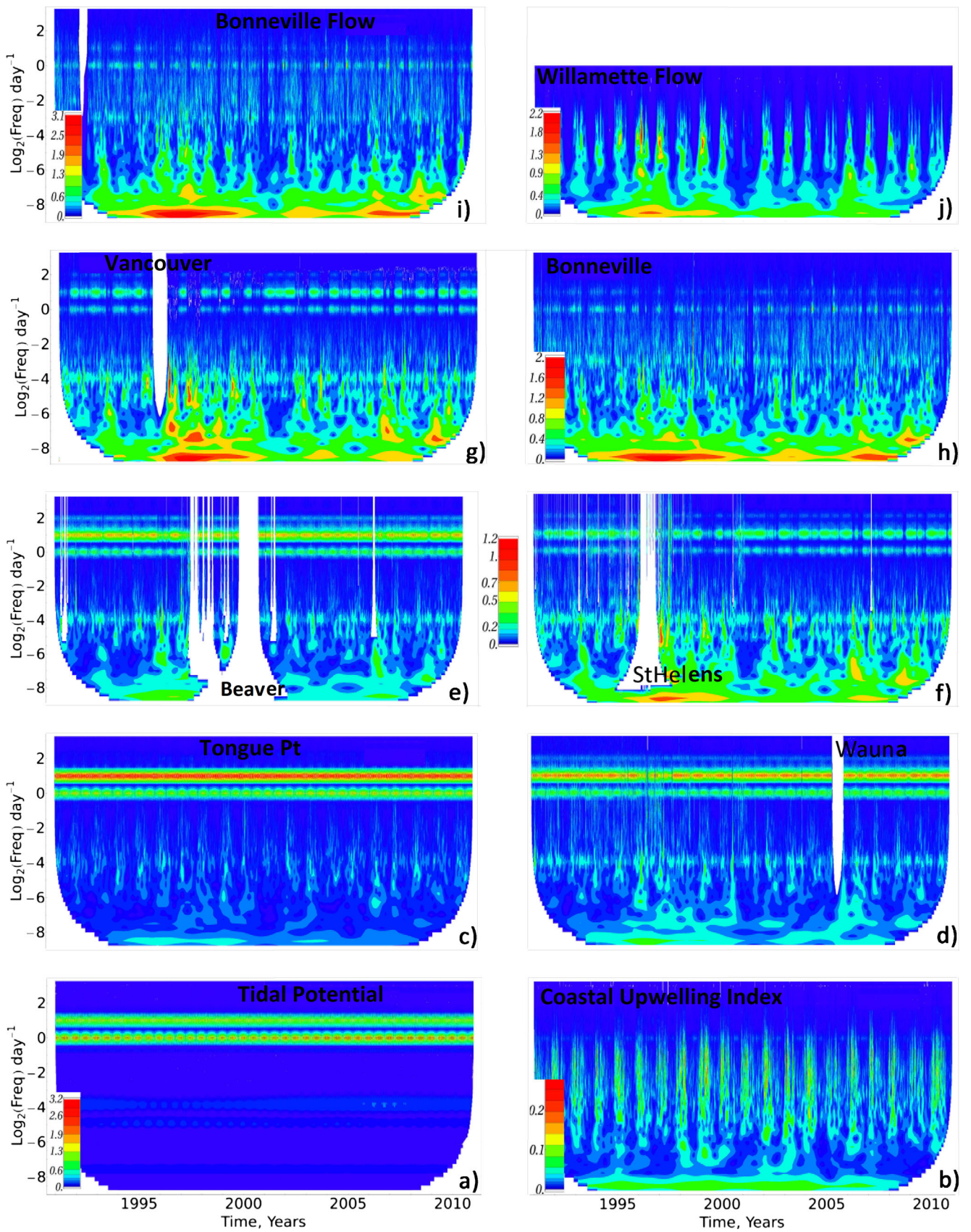
20 days each winter. It has much less energy than the Bonneville flow at periods at and above 7 days. The very dry winter of 2001 is more evident as a quiet period than in the Bonneville record, because of Bonneville power-peaking and other mainstem reservoir operations.

Floodplain Stations. Floodplain CWT amplitude scaleograms (Fig. 6a–f) are somewhat different from those for channel stations. The most important distinction is methodological— the 1-year LOR for these stations limits the longest period resolved to 30 days, limiting the frequency range plotted in Fig. 6. The D_1 and D_2 tidal signals are diminished relative to nearby channel stations due to truncation of low waters, but the degree of truncation is variable between floodplain

stations (e.g., extreme at CHM, much less at CSRM). Overtides (D_3 to D_8) are more prominent relative to D_1 and D_2 at the four more seaward floodplain stations (CHM; Ryan Island Marsh or RIM at rkm-61; CRM; and GIC), because of the distortion of the tidal wave as it moves into shallow water, and there is usually more energy in the 15-day neap-spring band (Fig. 6a–d). Weekly power-peaking is sporadically evident at all the floodplain stations from CRM landward (Fig. 6c–f), but especially at CSRM and HCM. Daily power-peaking is evident at HCM (Fig. 6f) during some periods. At HCM, a fall period of low Columbia River flow (about day 50 to day 100) and several periods thereafter are "quiet" with no tidal variability; during these periods, HCM is isolated from fluvial influences.
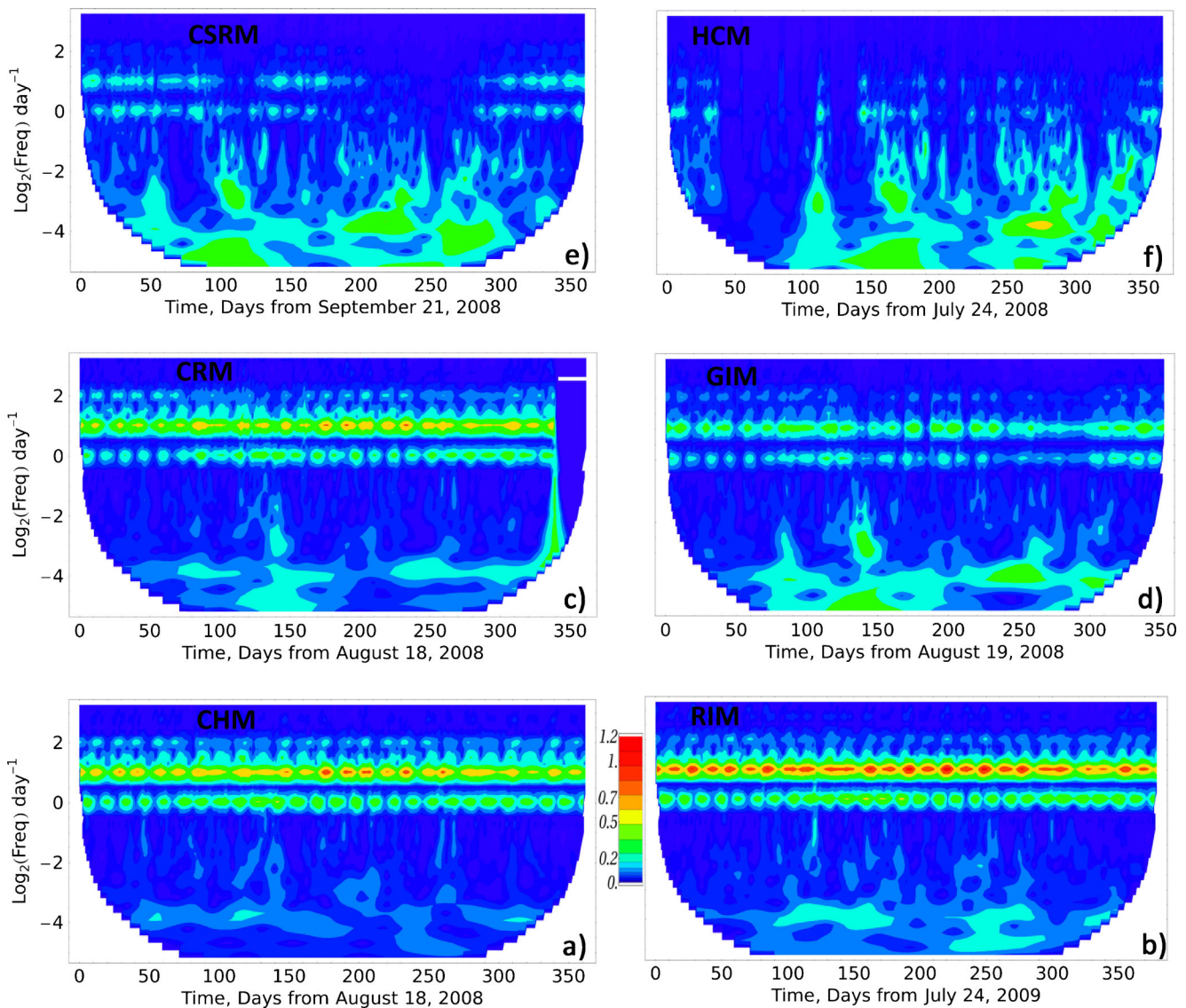

Fig. 6 Continuous wavelet transform (CWT) amplitude scaleograms (in m), 2008–2009, for selected floodplain stations: **a** Chinook River Marsh (CHM, rkm-12), **b** Ryan Island Marsh (RIM, rkm-61), **c** Clatskanie River Marsh (CRM, rkm-98), **d** Goat Island Marsh (GIC, rkm-131), **e** Current Sandy River Mouth (CSRM rkm-195), and **f** Hardy Creek Marsh (HCM, rkm-229)

Harmonic Analysis Results

Harmonic analysis provides a detailed view of the time-averaged frequency content at specific frequencies known to be associated with the tides. While the frequency resolution is very high for noise-free data with sharp frequency bands, frequency resolution is limited in practice by the presence of nontidal variance and time variations in tidal processes, both of which effectively broaden the peaks of the tidal spectrum so that they cannot always be separated (Munk and Hasselmann 1964).

Amplitudes. The lunar semidiurnal (D_2) constituent M_2 has an estuarine amplitude of ~0.95–0.98 m, is the largest tidal constituent, and is the largest factor in inundation of the floodplain of the system up to Beaver (Fig. 7). S_2 and N_2 are the second and third largest D_2 constituents, with estuarine amplitudes of ~0.24 and 0.18 m, respectively. The semidiurnals generally decrease landward, except that M_2 shows some amplification in the lower estuary. The ratio of N_2 to M_2 decreases upriver due to nonlinear friction—the impact of large constituents on a smaller constituent is larger than the impact of the small constituent on the larger ones. For reasons described in the next paragraph, the S_2 to M_2 amplitude ratio increases from rkm-170 landward due to power-peaking, such that S_2 is larger than M_2 at Bonneville. Floodplain D_2 constituent amplitudes (symbols in Fig. 7) generally follow channel trends closely.

K_1 is the largest diurnal constituent (Fig. 7); its amplitude in the estuary is ~0.45 m, less than half of that of M_2. Other diurnals are smaller, e.g., O_1 and P_1, the second and third largest diurnals. O_1 and K_1 generally decrease upriver, while P_1 initially decreases and then increases sharply landward of rkm-170. The ratio of O_1 to K_1 amplitudes decreases landward, as expected, because of nonlinear friction. The diel peak S_1 (with a period of exactly 24 h) is small in the estuary, because it is not prominent in the tidal potential. It increases upriver due to diel power-peaking; smaller increases in K_1 and P_1 occur at the landward end of the system for similar reasons. S_2 increases near Bonneville because it is effectively an overtide of S_1, associated with the sharp daily increases and decreases in flow. At Bonneville, M_2 is smaller than either S_1 or S_2, and the "tide" is a diel, not a diurnal, process. Floodplain diurnal constituent amplitudes generally follow those for channel stations, but K_1, P_1, and S_1 values are smaller at the landward end of the system, likely due to truncation of lower low waters at floodplain stations (symbols in Fig. 7). Because they represent the effect of lower low water, floodplain diurnals are more affected by truncation than semidiurnals.

Tidal wave propagation in a convergent estuary is a balance between "topographic funneling" (i.e., reduced cross-sectional area that concentrates energy and increases amplitudes), frictional energy loss, and nonlinear generation of overtides and tidal monthly variations (Jay 1991). The latter two processes reduce the amplitude of the major tidal constituents. The potential for funneling is limited in the LCRE, because channel cross-sectional area, controlled largely by a navigation channel, is nearly constant above Beaver. Still, friction increases landward because of high river-flow velocities and decreases amplitudes. Nonlinear friction transfers energy to overtides MK_3 (from interaction of M_2 with K_1) and M_4 (from the quadratic interaction of M_2 with itself) and to tidal monthly variations (e.g., to MSf with a period of 15 days, from the interaction of M_2 and S_2), increasing the amplitudes of these frequencies at the cost of the astronomical constituents.

Thus, amplitudes decrease in the landward direction for most astronomically forced constituents, e.g., K_1, O_1, M_2, S_2, and N_2 (Fig. 7). However, there is a local maximum in M_2, the largest constituent, at Tongue Point (rkm-29) due to wave reflection, as the estuary narrows at that point. This is not seen in the other constituents, because they are smaller than M_2; the combined friction of M_2 and river flow on them prevents amplification. As a consequence of the relatively slow decrease in M_2, the ratio of diurnal to semidiurnal (D_1/D_2) constituents decreases in the landward direction between the entrance and Wauna (rkm-68) for both channel and floodplain stations. Thereafter, the D_1/D_2 constituent ratio nearly doubles, due to power-peaking.

The overtides MK_3 and M_4 derive from frictional nonlinearities not astronomical forcing; they are very small in the estuary, but increase landward to a maximum at Beaver (Fig. 7). Energy transfer to overtides is limited, however, because of the landward decrease in amplitudes of the major constituents and the changing nature of the friction term as river flow increases. This explains the maximum in overtides in the lower tidal river and their subsequent decrease upriver. MSf shows a similar maximum, though further landward in the tidal river than the maximum in overtides. As noted by Giese and Jay (1989) and Buschman et al. (2010), MSf represents a tide-flow interaction—there is greater tidal friction on the flow during spring tides. In addition, there is an additional discharge on spring tides that compensates for the larger landward Stokes drift on springs. For both of these reasons, river slopes (therefore, upriver water levels) must be higher to discharge the same amount of water from land.

Finally, H_1 (a semidiurnal despite its name) increases from the entrance to Vancouver, before decreasing sharply (Fig. 7). As for MSf and S_1, the astronomical forcing for H_1 is very small. H_1 is, however, exactly 1 cycle year^{-1} lower in frequency than M_2, and it is the strong annual modulation of M_2 by river flow that causes H_1 to increase to a maximum at rkm-169. Constituent H_2 (not shown), which is 1 cycle year^{-1} higher in frequency than M_2, is slightly smaller than H_1, but has the same spatial pattern. Floodplain station results for H_1 are erratic, but are generally smaller in the upper tidal river, because of truncation of low waters. Floodplain MSf results
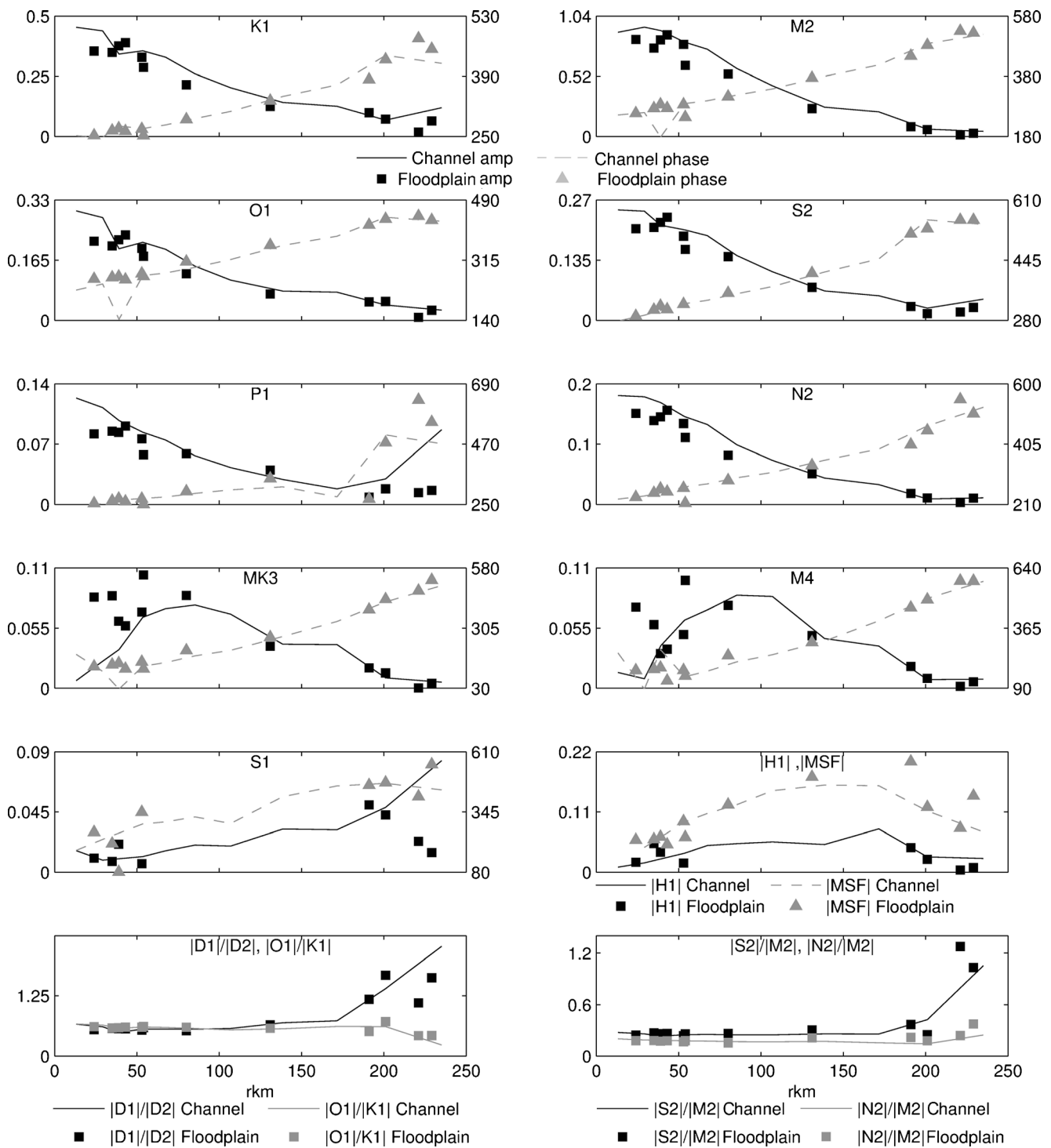
Fig. 7 Harmonic analysis results from a 1-year window: average amplitudes (*black*) and phases (*gray*) of selected constituents as a function of rkm for channel stations (*continuous curves*) and floodplain stations (*symbols*). D_1 constituents K_1, O_1, P_1, and S_1, overtide MK_3 and the D_1 to D_2 and O_1 to K_1 ratios are shown *at left*, with the D_2 constituents M_2, S_2, and N_2 and H_1, overtide M_4, the 15-day constituent MSf, and the S_2 to M_2 and N_2 to M_2 amplitude ratios are *at right*. Some constituents cannot be determined at all floodplain stations for statistical reasons

follow channel results in the estuary, reflecting the very large seasonal change in tidal conditions in this area. MSf is larger at floodplain than channel stations near Bonneville Dam, probably because tides are only present when water levels are high enough for there to be a large tidal monthly cycle.

Phases. Phases represent the timing of the tide and for most constituents increase in the landward direction, i.e., high water (the crest of the tidal wave) arrives later at upriver points because the astronomical tide propagates landward. For M_2, the phase change per hour is 360° divided by the period

(12.42 h), or 28.99°h^{-1}. The average M_2 phase change between Hammond (rkm-15) and Vancouver (rkm-169) is ~175° or ~6 h (Fig. 7). S_2 and N_2 propagation speeds are similar. For K_1 (period of 23.93 h), the phase change per hour is 15.04°h^{-1}. The corresponding time difference for K_1 is 149° or ~9.9 h; O_1 phases are similar, but S_1 phases are perturbed by power-peaking. The phases of MK_3 to M_4 both show a minimum in the estuary, before increasing upriver. These minima are associated with a shift in the nature of the overtides, from generation outside the estuary (or at the entrance) to generation by tidal-fluvial interactions. The actual high water propagation time, influenced by D_1, D_2, and overtides, varies with flow from ~8 to 12 h, with slower propagation during high-flow periods. The average propagation times to Bonneville for M_2 and K_1 are 9.4 and 20.1 h, respectively, but longer during high-flow periods. Thus, depending on flow, the length of the system from the ocean to Bonneville Dam is ~0.75–1 wavelength. (A wave travels a distance of one wavelength in one wave period.)

Separation of Variance

Plotting water level variance and the components thereof related to the major sources of external forcing provides further insight into the LCRE water level regime. Presented are variance in meters squared and as a percent of total channel variance (left- and right-hand columns, respectively) for channel and floodplain stations (Fig. 8). Total variance at all frequencies (Fig. 8a, b) generally increases from the ocean landward, but there is a broad minimum between rkm-68 and rkm-107. The maximum variance, at Bonneville (rkm-233), is ~2.5× the minimum. Total variance is lower at floodplain stations in part because of the clipping of low waters (especially in the estuary), but mostly because seasonal variance is not resolved with the short 1–2-year floodplain records (especially in the tidal river). In terms of the sources of variance discussed in the following paragraphs, floodplain stations show considerable irregularity. This is primarily related to local topography, but local tributary inflow may also play a role. The fact that the channel variance inferred from the CWT analysis is ~90–105 % of the original time-series variance (Fig. 8b) indicates that the variance overlap corrections described in ESM1c were effective.

Water level variance in the lower estuary and energy minimum zones up to Beaver is largely controlled by tidal daily processes, i.e., by the D_1 and D_2 tides (Fig. 8c, d). The maximum tidal variance occurs at Tongue Point, caused by a maximum in D_2 amplitude at rkm-20 to rkm-29. Tidal monthly energy is maximal in absolute terms at Reed Island (rkm-201), but accounts for the largest percentage of variance at St Helens (rkm-139). Overtide variance peaks in both relative and absolute terms at Longview, rkm-107.

Seasonal and fluvial variance increases ~30× between the estuary and Bonneville (rkm-233; Fig. 8e, f). In the estuary, tidal daily variance accounts for ~70 % of the total variance, while seasonal plus fluvial variance is 70–90 % of the total from Vancouver landward.

Power-peaking and weather-band energy are difficult to distinguish in terms of frequency. Analyses discussed in Part II suggest that power-peaking is small seaward of Beaver (rkm-87), while atmospheric effects are small landward of that point. Thus, the two were distinguished spatially (Fig. 8g, h). Neither ever accounts for >6 % of the total variance for floodplain stations or >2.5 % for channel stations. In absolute terms, however, power-peaking has as much or more variance than the daily tides landward of about rkm-200.

Discussion and Conclusions

Tidal-fluvial water levels in the LCRE are nonlinear, nonstationary, and influenced by a number of factors—astronomical tidal forcing, spatially variable channel width and depth, the presence (or absence) of peripheral intertidal areas, river flow, coastal processes (primarily upwelling and downwelling), and power-peaking. The focus of this analysis has been to provide an along-channel perspective on the issues of (a) how external forcing processes (river flow, astronomical tidal forcing, coastal upwelling and downwelling, and power-peaking) are reflected in system water levels; (b) why the water level spectrum varies in space-time; (c) how energy is transferred between different space and time scales; and (d) how floodplain stations differ from channel stations. To answer these questions, we have provided a spatially and spectrally comprehensive view of water level variations at channel and floodplain stations. Because LCRE processes are nonstationary and nonlinear, a variety of time-series analysis techniques—power spectra, continuous wavelet transforms, and harmonic analysis—were employed to understand time-space variations and energy transfers.

The importance of coastal processes, tidal forcing, and river flow all vary strongly along the channel. Water levels in the estuary (i.e., below rkm-87) are controlled primarily by daily (D_1 and D_2) tidal oscillations (>60 % of the variance), with some influence of coastal processes related to atmospheric pressure and winds. The fluvial contribution to estuarine variance is small. This is evident from the wavelet (CWT) and variance analyses. In the CWT scaleograms, most of the estuarine variance is in the horizontal bands associated with the D_1 and D_2 tides, directly reflecting the spectral content of astronomical tidal forcing. Coastal upwelling and downwelling (reflected in the CUI) exert considerable influence on estuarine water levels, but the importance of this influence decreases in the more landward parts of the system, both in absolute and percentage terms. This decrease is due
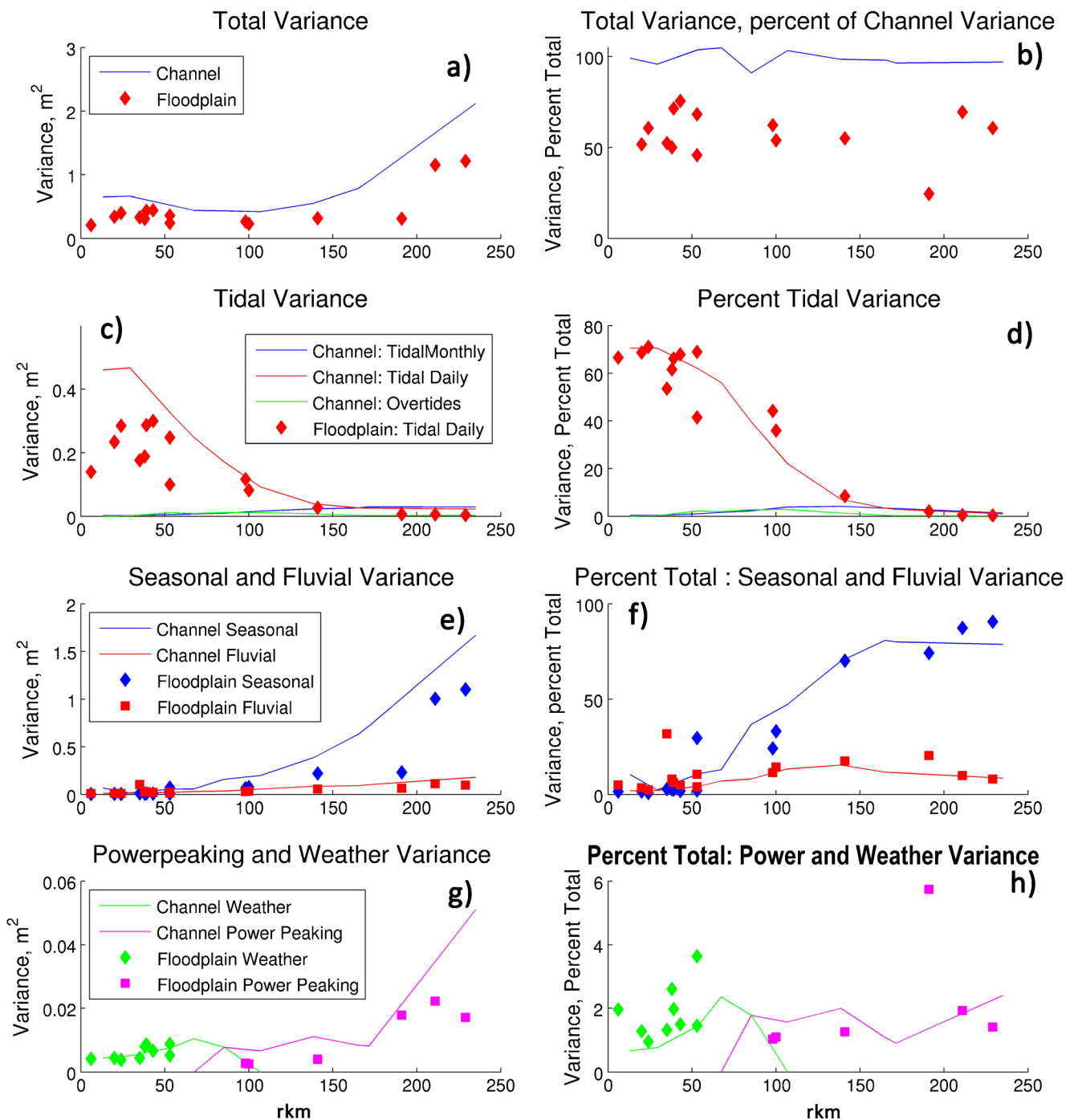
Fig. 8 Partition of variance for channel (*line*) and floodplain (*symbols*) in square meter (*left*) and as % total (*right*), as a function of along-channel distance (km). In **a** total variance; **b** % of original channel time series variance; **c, d** contributions of tidal components (tidal daily, overtide and tidal monthly, fluvial); **e, f** seasonal (periods >30 days) and fluvial (periods ≥30 days); and **g, h** power-peaking and weather-band variance

primarily to strong river flow friction on the wave-like elevation adjustment to coastal sea level as it propagates upriver. Tidal monthly and overtide variations in water level are weak in the estuary, but they increase in the landward direction, because of nonlinear, frictional energy transfer from the major tidal species. Tidal monthly energy is maximal between about rkm-140 and rkm-200. Tidal daily and coastal influences

decrease in the landward direction, while fluvial influences increase, accounting for 70–90 % of the variance landward of rkm-150. Further, local winds may oppose the influence of coastal processes. At the Bonneville gauge, tides and atmospheric effects are minor, and water level fluctuations are almost totally dominated by river-flow variations, both natural and human.

Wavelet (CWT) scaleograms are particularly useful for understanding time-space patterns of water levels. One of the clearest features of the LCRE water level regime is the spatial evolution between the ocean and Bonneville Dam (Fig. 5), from horizontal bands (nearly stationary processes) to vertical bands (event-like processes). The scaleogram for Tongue Point (rkm-29) shows a mostly horizontal pattern (reflecting nearly stationary tides and an annual coastal sea level cycle) with a smaller nonstationary coastal component appearing as vertical bands. In the more landward parts of the system, additional horizontal bands appear for overtides, tidal monthly variations, and power-peaking. However, vertical patterns reflecting event-like flow variations become much more prominent and dominate the scaleograms for the more landward stations.

Power spectra are useful in showing the average frequency content and the very "red" spectra (i.e., dominated by seasonal and annual river flow variations) of stations in the tidal river. The spectral signatures of river flow at Bonneville, the CUI, and the astronomical tidal potential are all seen in water level spectra. Harmonic analysis results show that the system is ~1 wavelength long, but that the effective wavelength and tidal propagation speeds vary with flow. The influence of power-peaking in providing a seaward-propagating diel (S_1) wave with an S_2 "overtide" is also revealed by the harmonic analysis. All three frequency domain representations show, in different ways, a landward increase of the modulation of the tides by river flow and the generation of nonlinear overtides and tidal-month variations, with maximums in the tidal river 70–150 km below Bonneville Dam.

The primary differences at floodplain stations relative to channel stations include the following: (1) truncation of low waters at almost all stations; (2) periodic isolation of stations in the upper part of the tidal river from the channel during low flow periods; (3) reduced tidal energy levels due to truncation and high friction, especially noticeable at stations like Chinook Marsh that have very high-elevation channel bottoms; and (d) very distorted tides, with the distortion varying according to the geometry of the station. Water level patterns at individual floodplain stations are quite diverse due to the variable degree of truncation and seasonal isolation (the latter a factor only at upriver stations). Factors contributing to diversity among the floodplain stations are as follows: site elevation, along-channel variability of the ratio of tidal range to amplitude of the annual flow cycle, and the types of vegetation and channel obstacles controlling the roughness. Forested wetlands occur throughout the system in locations without salinity intrusion (e.g., in bays peripheral to the estuary), and tides in forested (and previously forested) wetlands are especially diverse and variable because of the changing distribution of large wood in channels (Diefenderfer and Montgomery 2009).

Finally, water levels, water level variance, and the resulting inundation patterns are relevant factors for understanding floodplain vegetation, but water level variance should not be confused with flow energy. Water level variance shows (Fig. 8) a minimum at the lower end of the tidal river, from Beaver (rkm-87) to Longview (rkm-107). In contrast, Jay et al. (1990) found that the minimum in tidal + fluvial energy dissipation at the bed occurs in the broadest part of the estuary from rkm-15 to rkm-40. Tidal + fluvial energy dissipation (in watts m^{-2}) at Beaver is approximately four times as large as that in the lower estuary, even though the water level variance is lower at Beaver. Water level variance is low at Beaver, despite high dissipation, because most of the dissipation is due to fluvial currents, which vary slowly, relative to the tides.

The contribution of this study to the analysis of tidal rivers globally is twofold. On the methodological side, we have provided a comprehensive view of time-space variations in water levels in a major tidal river and estuary, the LCRE. Because of strong, multiscale time variability, strong along-channel gradients in processes, and lateral differences between channel and floodplain, it is vital to have long records from all parts of the system, including the mainstem river and floodplain channels. It is also important to analyze nonstationary processes with multiple tools, because no single tool is adequate and any single tool can be misleading—John Godfrey Saxe's image of the blind men and the elephant is apt. Power spectra provide detailed resolution in frequency space, but little indication regarding time variations in frequency content. CWTs resolve time variations of frequency content, but less frequency resolution than is needed. Harmonic analyses are interpretable, but the anomalous results mentioned above for H_1, for example, can be viewed as demonstrating methodological problems as much as they illustrate the physics of the system. On the whole, the complexity of LCRE processes is likely representative—large tidal rivers will almost universally exhibit similar intricacies when viewed using the frequency domain representations employed here.

Our contribution on the process side is to illuminate the poorly understood transition from coastal and tidal to fluvial forcing that all large tidal rivers exhibit, though the spatial details of the variance distribution between processes will vary, and not all will show artificial processes like power-peaking. The transition seen in the LCRE from sharp tidal peaks (perturbed only slightly by coastal and fluvial processes) to broad seasonal and diel peaks (the latter only if power-peaking is present) is likely present in most tidal rivers. Finally, we have also demonstrated that water level fluctuations due to power-peaking propagate and can cause changes in the tidal regime for long distances, ~150 km in this case. These results provide a basis for understanding the distribution of wetlands in the LCRE (in Part II) and elsewhere.

References

Amin, M. 1983. On perturbations of harmonic constants in the Thames estuary. *Geophysical Journal Royal Astronomical Society* 73: 587–603.

Amphlett, M.B., T.E.Brabben, 1991. Measuring freshwater flows in large tidal rivers. In: Braga, Jr., B.P.F., Fernandez-Jauregui, C.A. [Eds] Water management of the Amazon Basin Manaus 5-9, 1990. UNESCO, Montevideo, pp. 179-190.

Barendregt, A., D. Whigham, and A. Baldwin (eds.). 2009. *Tidal freshwater wetlands*. Leiden: Backhuys Publishers.

Bezerra, M.O.M., R. Pontes, M.N. Gallo, A.M.C. Carmo, S.B. Vinzon, and R.P. Rosario. 2008. Forcing and mixing processes in the Amazon estuary: a study case. *Nuovo Cimento- Societa Italiana di Fisica Sezione C* 31: 743–756.

Borde, A.B., V.I. Cullinan, H.L. Diefenderfer, R.M. Thom, R.M. Kaufmann, J. Sagar, and C. Corbett. 2012. *Lower Columbia River and Estuary Ecosystem Restoration Program Reference Site Study: 2011 restoration analysis*. Prepared for the Lower Columbia River Estuary Partnership by Pacific Northwest National Laboratory.

Bunn, S.E., and A.H. Arthington. 2002. Basic principles and ecological consequences of altered flow regimes for aquatic biodiversity. *Environmental Management* 30: 492–507.

Buschman, F.A., A.J.F. Hoitink, M. van der Vegt, and P. Hoekstra. 2010. Subtidal flow division at a shallow tidal junction, *Water Resources. Research.* 46, W12515. doi:10.1029/ 2010WR009266.

Cartwright, D.E., and A.C. Edden. 1973. Corrected tables of tidal harmonics. *Geophysics Journal of the Royal Astronomical Society* 33: 253–264.

Castaing, P., and G.P. Allen. 1981. Mechanisms controlling seaward escape of suspended sediment from the Gironde: a macrotidal estuary in France. *Marine Geology* 40: 101–118.

Diefenderfer, H.L., and D.R. Montgomery. 2009. Pool spacing, channel morphology, and the restoration of tidal forested wetlands of the Columbia River, U.S.A. *Restoration Ecology* 17: 158–168.

DiLorenzo, J.L., P. Huang, M.L.Thatcher, and T.O. Najarian. 1993. Dredging impacts of Delaware estuary tides, *Estuarine and Coastal Modeling III: Proceedings of the 3rd International Conference*, pp. 86−104.

Emery, W.J., and R.E. Thomson. 1997. *Data analysis methods in physical oceanography*. New York: Pergamon Press. 634pp.

Flinchem, E.P., and D.A. Jay. 2000. An introduction to wavelet transform tidal analysis methods. *Estuarine, Coastal and Shelf Science* 51: 177–200.

Gallo, Marcos, and Susana Vinzon. 2005. Generation of overtides and compound tides in Amazon estuary. *Ocean Dynamics* 55: 5–6.

Giese, B.S., and D.A. Jay. 1989. Modeling tidal energetics of the Columbia River Estuary. *Estuarine, Coastal and Shelf Science* 29: 549–571.

Godin, G. 1999. The propagation of tides up rivers with special considerations on the upper Saint Lawrence River. *Estuarine, Coastal and Shelf Science* 48: 307–324.

Gowing, D.J., and G. Spoor. 1998. *United Kingdom floodplains*, eds. R. Bailey, P. Jose, and B. Sherwood, 185-196. Otley, United Kingdom, Westbury Academic and Scientific Publishing.

Hida, N., J.G. Maia, O. Shimmi, M. Hiraoka, and N. Mizutani. 1998. Annual and daily changes of river water level at Breves and Caxiuana, Amazon Estuary. *Geographical Review of Japan Series B* 71: 100–105.

Horrevoets, A.C., H.H.G. Savenije, J.N. Schuurman, and S. Graas. 2004. The influence of river discharge on tidal damping in alluvial estuaries. *Journal of Hydrology* 294: 213–228. doi:10.1016/j.jhydrol.2004.02.012.

Huber, P. J., 1996. Robust statistical procedures, 2nd Ed. No. 68 in CBMS-NSF Regional Conference Series in Applied Mathematics Society of Industrial and Applied Mathematics.

Jay, D.A. 1991. Green's law revisited: tidal long wave propagation in channels with strong topography. *Journal of Geophysical Research* 96: 20,585–20,598.

Jay, D.A., and E.P. Flinchem. 1997. Interaction of fluctuating river flow with a barotropic tide: a test of wavelet tidal analysis methods. *Journal of Geophysical Research* 102: 5705–5720.

Jay, D.A., and E.P. Flinchem. 1999. A comparison of methods for analysis of tidal records containing multi-scale non-tidal background energy. *Continental Shelf Research* 19: 1695–1732.

Jay, D.A., B.S. Giese, and C.R. Sherwood. 1990. Energetics and sedimentary processes in the Columbia River Estuary. *Progress in Oceanography* 25: 157–174.

Jay, D.A., K. Leffler, and S. Degens. 2011. Long-term evolution of Columbia River tides. *Journal of Waterway, Port, Coastal, and Ocean Engineering* 137: 182–191. doi:10.1061/(ASCE)WW.1943-5460.0000082.

Jay, D.A., and P. Naik. 2011. Distinguishing human and climate influences on hydrological disturbance processes in the Columbia River, USA. *Hydrological Sciences Journal* 56: 1186–1209.

Jay, D.A., and J.D. Smith. 1990. Circulation, density distribution and neap-spring transitions in the Columbia River Estuary. *Progress in Oceanography* 25: 81–112.

Jiao, N., Y. Zhao, T. Luo, and X. Wang. 2006. Natural and anthropogenic forcing on the dynamics of virioplankton in the Yangtze River estuary. *Journal of the Marine Biological Association of the United Kingdom* 86: 543–550.

Junk, W.J., and K.M. Wantzen. 2004. The flood pulse concept: new aspects, approaches and applications—an update. In: Welcomme, R.L., Petr, T. [Eds] Proceedings of the second international symposium on the management of large rivers for fisheries volume II: sustaining livelihoods and biodiversity in the new millennium, Phnom Penh, 11-14 February 2003. RAP Publication 2004/17. Food and Agriculture Organization of the United Nations, Bangkok, pp.117-140.

Kostachuk, R. 2002. Flow and sediment dynamics in migrating salinity intrusions: Fraser River Estuary, Canada. *Estuaries* 25: 197–203.

Kukulka, T., and D.A. Jay. 2003a. Impacts of Columbia River discharge on salmonid habitat I. A non-stationary fluvial tide model. *Journal of Geophysical Research* 108: 3293. doi:10.1029/2002JC001382.

Kukulka, T., and D.A. Jay. 2003b. Impacts of Columbia River discharge on salmonid habitat II. Changes in shallow-water habitat. *Journal of Geophysical Research* 108: 3294. doi:10.1029/2003JC001829.

LeBlond, P.H. 1978. On tidal propagation in shallow rivers. *Journal of Geophysical Research* 83: 4717–4721.

Leffler, K., and D.A. Jay. 2009. enhancing tidal harmonic analysis: robust (hybrid L1/L2) solutions. *Continental Shelf Research* 29: 78–88.

Levings, C.D., K. Conlin, and B. Raymond. 1991. Intertidal habitats used by juvenile Chinook salmon (*Oncorhynchus tshawytscha*) rearing in the north arm of the Fraser River estuary. *Marine Pollution Bulletin* 22: 20–26.

Mikhailova, M.V., and M.V. Isupova. 2006. Water circulation, sediment dynamics, erosional and accumulative processes in the Gironde Estuary (France). *Water Research* 33: 10–23.

Munk, W.H., and K. Hasselmann. 1964. Super-resolution of tides, in Studies in Oceanography (Hidaka Volume). Tokyo, pp. 339–344.

Naik, P.K., and D.A. Jay. 2005. Virgin flow estimation of the Columbia River (1879-1928). *Hydrologic Processes* 19: 1807–1824. doi:10.1002/hyp.5636.

Naik, P.K., and D.A. Jay. 2011. Distinguishing human and climate influences on the Columbia River: changes in mean flow and sediment transport. *Journal of Hydrology* 404: 259–277.

Nittrouer, J.A., J. Shaw, M.P. Lamb, and D. Mohrig. 2012. Spatial and temporal trends for water-flow velocity and bed-material sediment transport in the lower Mississippi River. *GSA Bulletin* 124: 400–414. doi:10.1130/B30497.1.

Pawlowicz, R., R. Beardsley, and S. Lentz. 2002. Classical tidal harmonic analysis with errors in Matlab using T-Tide. *Computers and Geosciences* 28: 929–937.

Parker, B. B., 1991. The relative importance of the various nonlinear mechanisms in a wide range of tidal interactions. In: *Progress in Tidal Hydrodynamics*, Ed. by B. B. Parker, John Wiley, pp. 237-268.

Sagar, J.P., A.B. Borde, L.L. Johnson, C.A. Corbett, J. L. Morace, K.H. Macneale, et al. 2013. Juvenile salmon ecology in tidal freshwater wetlands of the lower Columbia River and Estuary: Synthesis of the ecosystem monitoring program, 2005-2010. Portland: Lower Columbia Estuary Partnership.

Sassi, M. G., A. Hoitink, B. de Brye, B. Vermeulen, and E. Deleersnijder (2011), Tidal impact on the division of river discharge over distributary channels in the Mahakam Delta, Ocean Dynamics, 61: 2211–2228. doi:10.1007/s10236-011-0473-9.

Sherwood, C.R., D.A. Jay, R.B. Harvey, P. Hamilton, and C.A. Simenstad. 1990. Historical changes in the Columbia River estuary. *Progress in Oceanography* 25: 299–352.

Simenstad, C.A., J.L. Burke, J.E. O'Connor, C. Cannon, D.W. Heatwole, M.F. Ramirez, I.R. Waite, T.D. Counihan, and K.L. Jones. 2011.

Columbia River Estuary ecosystem classification—concept and application. U.S. Geological Survey Open-File Report 2011-1228, 60 p.

Smith, J.P., C.R. Olsen, T.D. Bullen, and D.J. Brabander. 2009. Strontium isotope record of seasonal scale variations in sediment sources and accumulation in low-energy, subtidal areas of the lower Hudson River estuary. *Chemical Geology* 264: 375–384.

Stronach, J.A., and T.S. Murty. 1989. Nonlinear river-tidal interactions in the Fraser River, Canada. *Marine Geodesy.* 13: 313–339.

Welcome, R.L. 1979. *Fisheries ecology of floodplain rivers*. New York: Longman.

White, M.A., J.C. Schmidt, and D.J. Topping. 2005. Application of wavelet analysis for monitoring the hydrologic effects of dam operation: Glen Canyon dam and the Colorado River at Lees Ferry, Arizona. *River Research and Applications* 21: 551–565.

Wiele, S.M., and J.D. Smith. 1996. A reach averaged model of diurnal discharge wave pro pagation down the Colorado River through the Grand Canyon. *Water Resources Research* 32: 1375–1386.

Wolanski, E. 2007. *Estuarine ecohydrology*. Amsterdam: Elsevier.

Yixin, Y., X. Fumin, and M. Lihua. 2001. Analysis of hydrodynamic mechanics for the change of the lower-section of the Jiuduan Sandbank in the Yangtze River Estuary. *Proceedings of the congress-international association for hydraulic research Conf* 29: 179–186.

Zolezzi, G.A., M.C. Bellin, B. Maiolini Bruno, and A. Siviglia. 2009. Assessing hydrological alterations at multiple temporal scales: Adige River, Italy. *Water Resources Research* 45:W12421. doi:10.1029/2008WR007266.